Electronic Supplementary Material (ESI) for New Journal of Chemistry.

Supporting Information

Tuning multichannel conductance via through-space conjugated naphthalene

Tianwei Li,[a] Luqing Gan,[a] Lin Li,[a]* Shijie Zhen[a]*

[a] Guangxi Key Laboratory of Electrochemical and Magneto-chemical Functional Materials, College of Chemistry and Bioengineering, Guilin University of Technology, Guilin 541006, P. R. China

* Corresponding author

E-mail address: zhenshijie1211@163.com

Table of Contents

1. General Information

NMR spectra were recorded on a Bruker AV 500 spectrometer. Single crystal X-ray diffraction intensity data were acquired in the Bruker-Nonices Smart Apex CCD diffractometer with graphite monochromatic CuKa radiation. UV/Vis absorption spectra were recorded on Shimazu UV-2600 spectrophotometer and fluorescence spectra were recorded on Horiba Fluoromax-4 fluorescence spectrophotometer. At the base set level of 6-31G (d, p), the ground state geometry is optimized using the density function with the B3LYP mixture function and the Gaussian 16 program[1]. Based on the obtained data from G16, molecular frontier orbital amplitude plot analysis are conducted by Multiwfn package[2]. Compounds **1, 2, 5, 6** and **7** were purchased from Energy Chemical (Shanghai). All reagents and drugs were sealed and not treated before use. All other chemicals and reagents were purchased from commercial sources and used as received without further purification.

2. Conductance Measurement and Data Analysis

The conductance measurement was carried out on a self-made STM-BJ device. Prior to measurement, the gold-coated substrates were cleaned by a piranha solution and then used as a gold tip a 0.25mm gold wire annealed in a butane flame. In the STM-BJ experiment, 0.1 mM of the target molecular solution dissolved in a solvent of 1,3, 5-trimethylbenzene (TMB) was dripped onto a gold-coated substrate, and the gold tip was controlled by a stepper motor and piezoelectric stack. The bias is maintained at 100 mV and the sampling rate is 20 kHz during repeated disconnection. During the measurement, thousands (>3000) of individual individual traces were recorded in each experiment and a one-dimensional conductivity histogram was constructed by collecting all the individual traces to determine the conductivity value. Meanwhile, we drafted the two-dimensional histograms by overlapping each individual trace to provide additional information of stretching distance.

3. Flicker noise analysis

In scintillation noise analysis experiments, the connection delay stops at about 150 ms where molecular coupling is likely to form. The conductivity value is obtained from the one-dimensional

conductivity histogram, and then the discrete Fourier transform is performed on the conductivity, and the data square is transformed to convert the conduction-time into the signal spectrum. The noise spectrum of each channel is obtained by setting sampling points over 5000 experiments.

To quantify the PSD, integrating the PSD from 100 to 1000 Hz, and normalized by the average conductance from the cut-out conductance step. Then, according to the two-dimensional histogram of normalized scintillation noise power and average conductance power, two-dimensional Gaussian surface fitting is carried out to change the flash noise power index and minimize the correlation between them. The equation of 2D Gaussian surface fitting are as follows:

$$f(x,y) = Ae^{[-\frac{(x-x_0)^2}{2\sigma_x^2} - \frac{(y-y_0)^2}{2\sigma_y^2}]}$$

The noise power is proportional to G^n where n is the scaling exponent. To further analysis of transport mode, we studied the relationship between conductance and noise power by fitting the scaling exponent of flicker noise in molecular junctions. We used conjugate gradient methods in Matlab curve fitting toolbox to get the parameters of Gaussian distribution and fit the 2D histogram of normalized flicker noise power and average conductance. The equation can be transformed as follows:

$$f(x,y) = Ae^{ax^2 + bxy + cx + dy + ey^2 + f}$$

The parameter b represents the correlation between the two variables x and y. We set y as the noise power, and x is the scaling n of G. N varies from 1 to 2 in the step of 0.1 when b is close to zero, the corresponding n is the scaling exponent of flicker noise, which gets the zero correlation between G and noise power. The two-dimensional histograms of normalized flicker noise power versus average conductance are plotted.[5,6]

4. Synthesis and Characterization

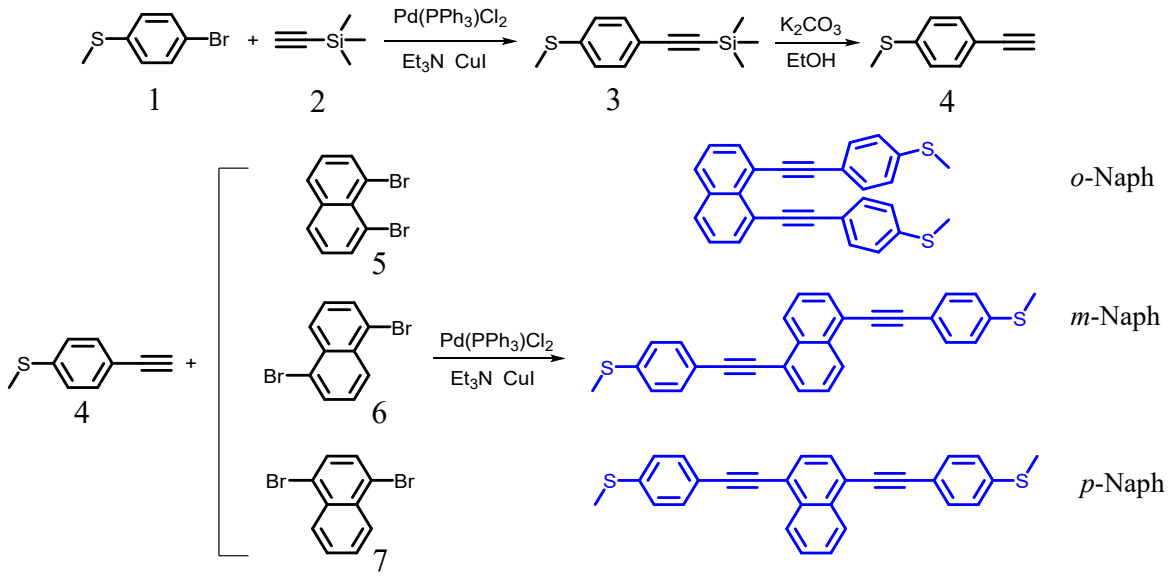

Scheme S1. Synthetic routes to *o*-Naph, *m*-Naph and *p*-Naph

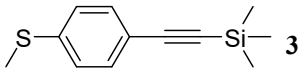

3

Trimethyl((4-(methylthio)phenyl)ethynyl)silane (3): 4-bromoanisole (**1**) (2.3 g, 10 mmol), triphenylphosphine palladium dichloride (0.7 g, 1 mmol) and cuprous iodide (0.19 g, 1 mmol) were added into a 250 ml two-necked round bottom flask. The flask was evacuated under vacuum and flushed with dry nitrogen three times and 4.5 mL trimethylsilylacetylene (**2**) (30 mmol) was added. After that, 150ml triethylamine bubbled in nitrogen was added, The reaction mixture was refluxed for 12 h. After cooling to room temperature, the crude product was purified by silica-gel column chromatography with PE. Yellow oily of **3** was obtained in 86% yield (1.89 g). ^{1}H NMR (500 MHz, $CDCl_3$), δ (ppm): 7.37 (d, J = 8.50 Hz, 2H), 7.15 (d, J = 8.50 Hz, 2H), 2.47 (s, 3H), 0.25 (s, 9H).

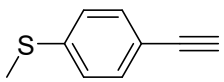

4

(4-ethynylphenyl)(methyl)sulfane (**4**): The intermediate product (**3**) (1.89 g, 8.6 mmol) was placed in a 250 ml round-bottomed flask with potassium carbonate (0.55 g, 4 mmol) and 100 ml methanol, and stirred at room temperature for 6 hours. The product was poured into water and extracted three

times with methylene chloride. The yield of yellow oily product was 97% (1.23 g). ^{1}H NMR (500 MHz, $CDCl_3$), δ (ppm): 7.42 (d, J = 8.50 Hz, 2H), 7.20 (d, J = 8.55 Hz, 2H), 3.10 (s, 1H).

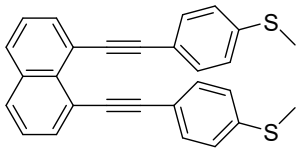

o-Naph

1,8-Bis((4-(methylthio)phenyl)ethynyl)naphthalene (*o*-Naph): 1,8-Dibromonaphtalene (**5**) (280 mg, 1 mmol), (4-ethynylphenyl)(methyl)sulfane (4) (450 mg, 3 mmol), triphenylphosphine palladium dichloride (35 mg, 0.05 mmol) and cuprous iodide (20 mg, 0.1 mmol) were added into a 125 ml two-necked round bottom flask. The flask was evacuated under vacuum and flushed with dry nitrogen three times and the reaction mixture was refluxed for 24 hAfter cooling to room temperature, the crude product was purified by silica-gel column chromatography with PE and DCM as eluent (v / v = 6 / 1) and yellow solid of *o*-Naph was isolated in 44% yield (0.186 mg). ^{1}H NMR (500 MHz, $CDCl_3$), δ (ppm): 7.84 (t, J = 8.15 Hz, 4H), 7.46 (t, J = 7.50 Hz, 2H), 7.23 (d, J = 8.30 Hz, 4H), 6.98 (d, J = 8.3 Hz, 4H), 2.46 (s, 6H). ^{13}C NMR (125 MHz, $CDCl_3$) δ 138.78, 134.70, 134.14, 131.78, 129.58, 125.58, 125.42, 120.83, 120.09, 96.39, 89.84, 15.39. HRMS ($C_{28}H_{20}S_2$): *m/z* 420.59 (M^+, calcd 420.10).

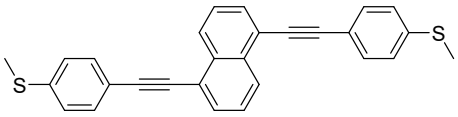

m-Naph

1,5-bis((4-(methylthio)phenyl)ethynyl)naphthalene (*m*-Naph): The procedure was analogous to that described as *o*-Naph and the reactants are 1,5-dibromonaphthalene (6) (280 mg, 1 mmol), (4-ethynylphenyl)(methyl)sulfane (4) (450 mg, 3 mmol), triphenylphosphine palladium dichloride (35 mg, 0.05 mmol) and cuprous iodide (20 mg, 0.1 mmol). White solid of *m*-Naph was isolated in 44% (0.189 g). ^{1}H NMR (500 MHz, $CDCl_3$), δ (ppm): 8.45 (d, J = 8.4 Hz, 2H), 8.27 (d, J = 7.35 Hz, 2H), 7.84-7.79 (m, 4H), 7.58-7.54 (m, 4H), 7.43 (t, J = 8.7 Hz, 2H), 2.55 (s, 6H). ^{13}C NMR (125 MHz, $CDCl_3$) δ 139.86, 134.47, 131.92, 131.86, 131.05, 130.59, 131.38, 127.78, 126.95, 126.68, 126.30,

125.91, 123.24, 121.59, 119.31, 94.72, 87.13, 15.38. HRMS ($C_{28}H_{20}S_2$): *m/z* 420.59 (M^+, calcd 420.10).

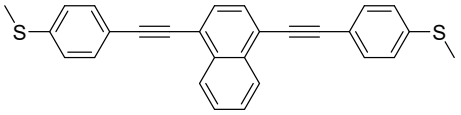

p-Naph

1,4-bis((4-(methylthio)phenyl)ethynyl)naphthalene (*p*-Naph): The procedure was analogous to that described as o-Naph and the reactants are 1,4-dibromonaphthalene (6) (280 mg, 1 mmol), (4-ethynylphenyl)(methyl)sulfane (4) (450 mg, 3 mmol), triphenylphosphine palladium dichloride (35 mg, 0.05 mmol) and cuprous iodide (20 mg, 0.1 mmol). White solid of m-Naph was isolated in 44% (0.187 g).. ^{1}H NMR (500 MHz, $CDCl_3$), δ (ppm): 8.45 (d, J = 9.1 Hz, 2H), 7.68 (d, J = 8.56 Hz, 2H), 7.67 (t, J = 3.1 Hz, 2H), 7.58 (d, J = 8.3 Hz, 4H), 7.28 (d, J = 4.45 Hz, 4H), 2.52 (s, 6H). ^{13}C NMR (125 MHz, $CDCl_3$) δ 139.82, 133.01, 131.94, 129.61, 127.22, 126.63, 125.91, 121.45, 119.42, 95.86, 87.69, 15.37. HRMS ($C_{42}H_{32}S_3$): *m/z* 420.59 (M^+, calcd 420.10).

5. X-Ray Crystallography

Crystal data for *o*-Naph (CCDC: 2235364): $C_{28}H_{20}S_2$, M_W = 420.10, triclinic, P-1, a = 14.2355(7) Å, b = 20.1323(6) Å, c = 23.7245(6) Å, α = 82.264(2)°, β = 78.9101(3)°, γ = 89.961(3)°, V = 6609.4(4) Å^3, Z = 1, Dc = 1.268 g cm^{-3}, μ = 2.264 mm^{-1} (MoKα, λ = 1.54178), F(000) =2640, T = 293(2) K, $2\theta_{max}$ = 67.679° (98.6%), 70109 measured reflections, 30155 independent reflections (R_{int} = 0.0478), GOF on F^2 = 1.747, R_1 = 0.2595, wR_2 = 0.5525 (all data), Δe 3.602 and −1.355 eÅ^{-3}.

6. Transmission Calculation

All the molecules are optimized based on the procedure described above, and making sure there is no imaginary frequency existed in the finally adopted structures. The molecules were then inserted between the Au electrodes to build up model devices by the Atomistic Tool Kit (ATK) software. The molecular junction was formed by semi-finite left and right electrodes (LE and RE, respectively) and a scattering region where the molecule was settled. A scattering region also comprises screening layers of LE and RE. The molecular device was examined using the Au (111) electrodes (both LE

and RE). The Au electrodes were settled to a 6*7*3 supercell. First, isolated organic molecules were optimized. After the optimization, organic molecules were inserted between the LE and RE, and the distance between the LE and RE was relaxed until the total energy reached minimum. Next, constraining the Au electrodes, organic molecules were relaxed. During the relaxation, the force tolerance was set to 0.05 eV/Å. Then, first principles calculations were carried out to expose the electronic transport properties. In calculations, the exchange-correlation potential was approximated within the generalized gradient approximation (GGA) with Perdew-BurkeErnzerhof (PBE) functional (GGA.PBE), for the exchange and correlation effects of the electrons. Double-ζ plus polarization (DZP) basis set for the molecule and single-ζ plus polarization (SZP) basis set for the electrodes. For geometry optimization, 1 k-point for x-, y- directions, and 50 k-points for z-direction, for transmission spectra and transmission pathways calculation, 3 k-point for x-, y- directions, and 100 k-points for z-direction.

7. Additional Spectra

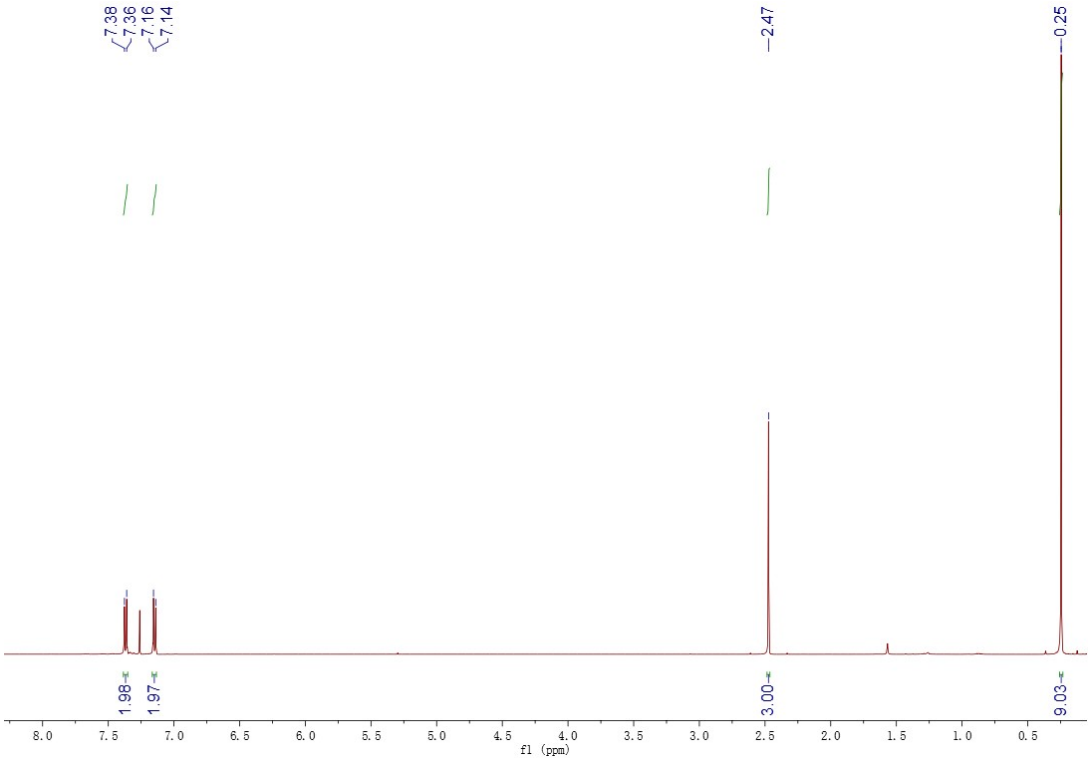

Figure S1. ^{1}H NMR spectrum of **3** in $CDCl_3$.

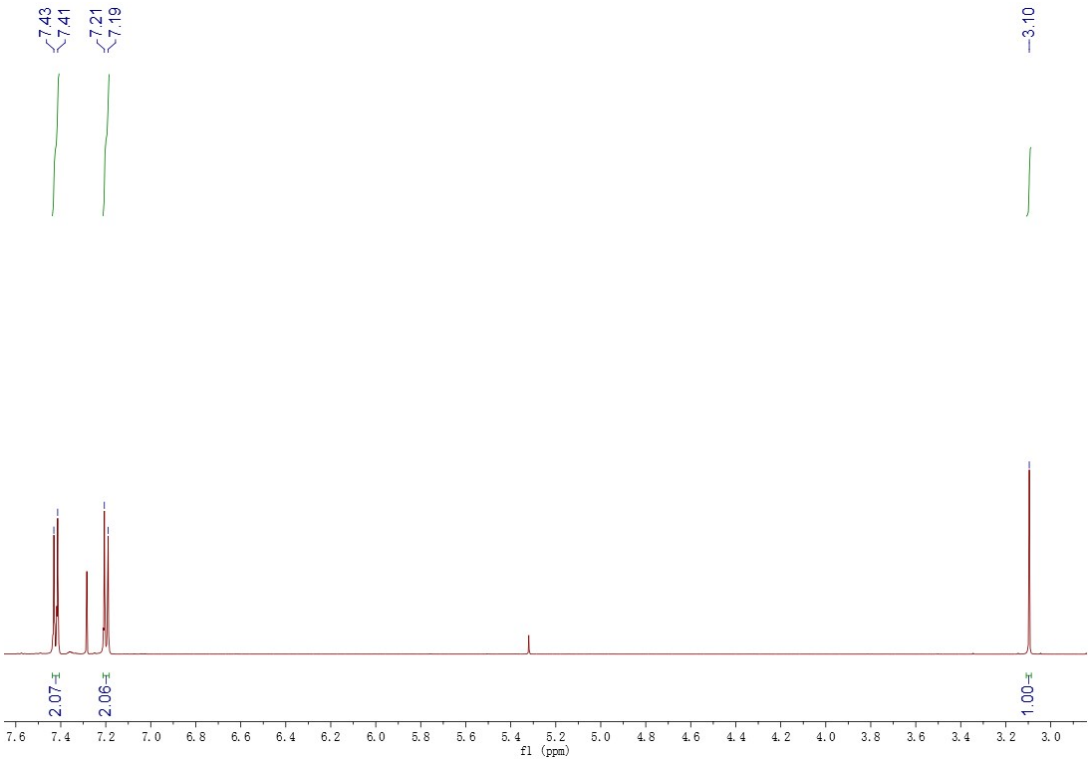

Figure S2. ^{1}H NMR spectrum of **4** in $CDCl_3$.

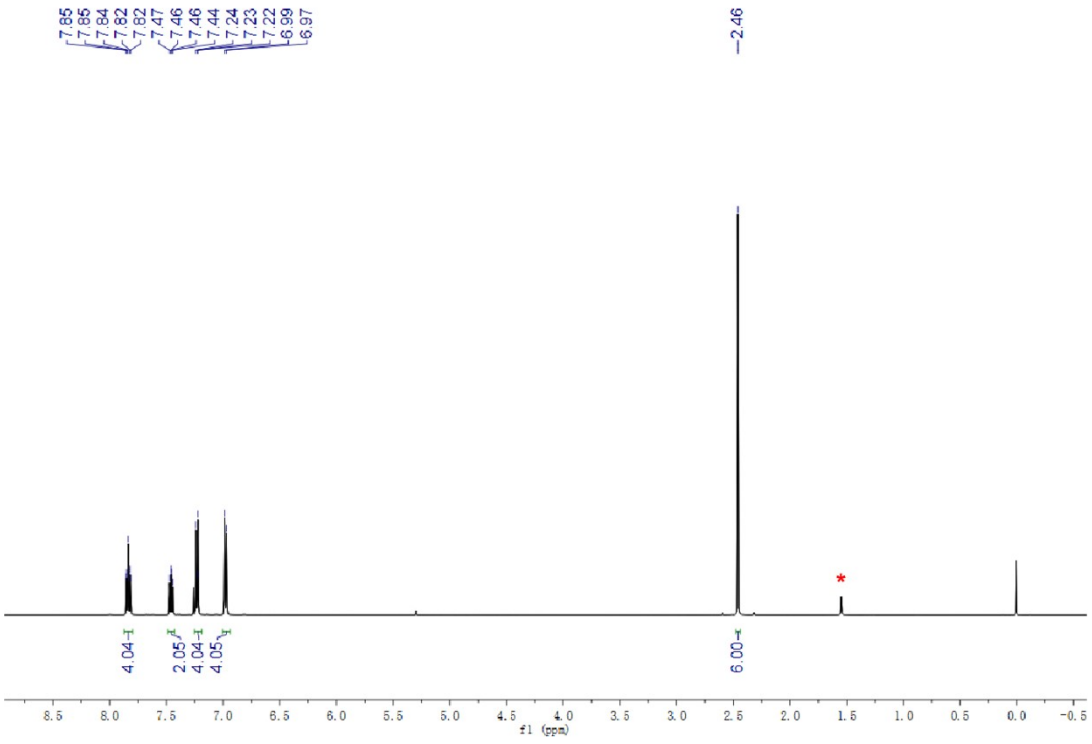

Figure S3. ^{1}H NMR spectrum of *o*-Naph in $CDCl_3$.

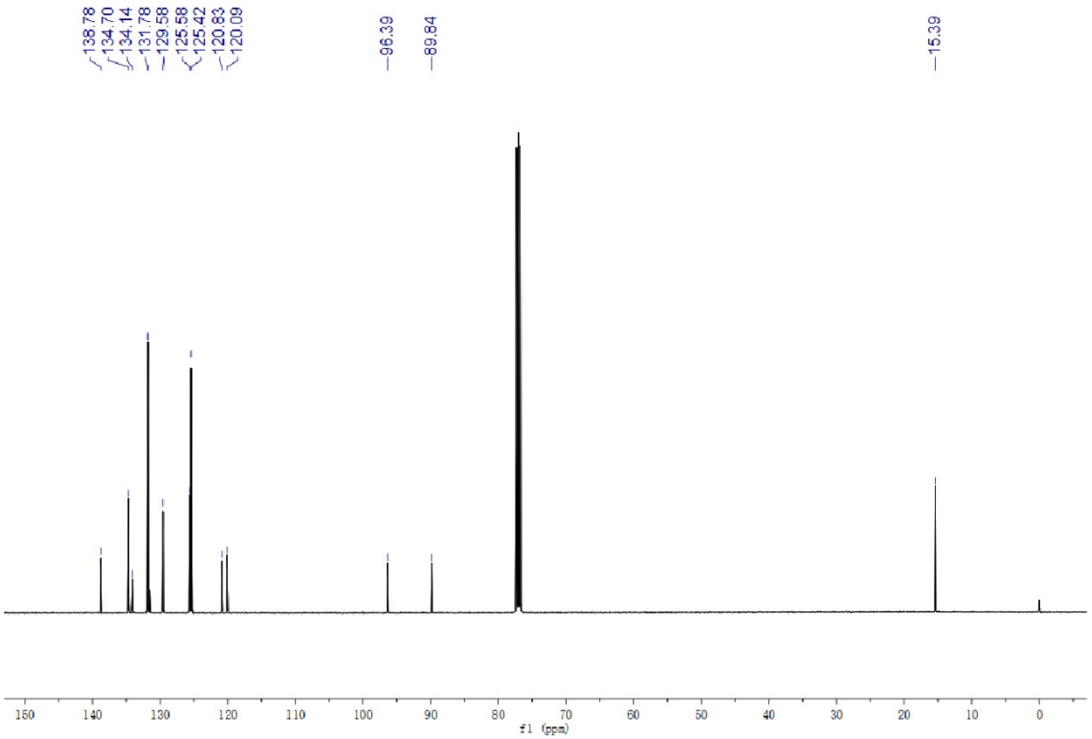

Figure S4. ^{13}C NMR spectrum of *o*-Naph in $CDCl_3$.

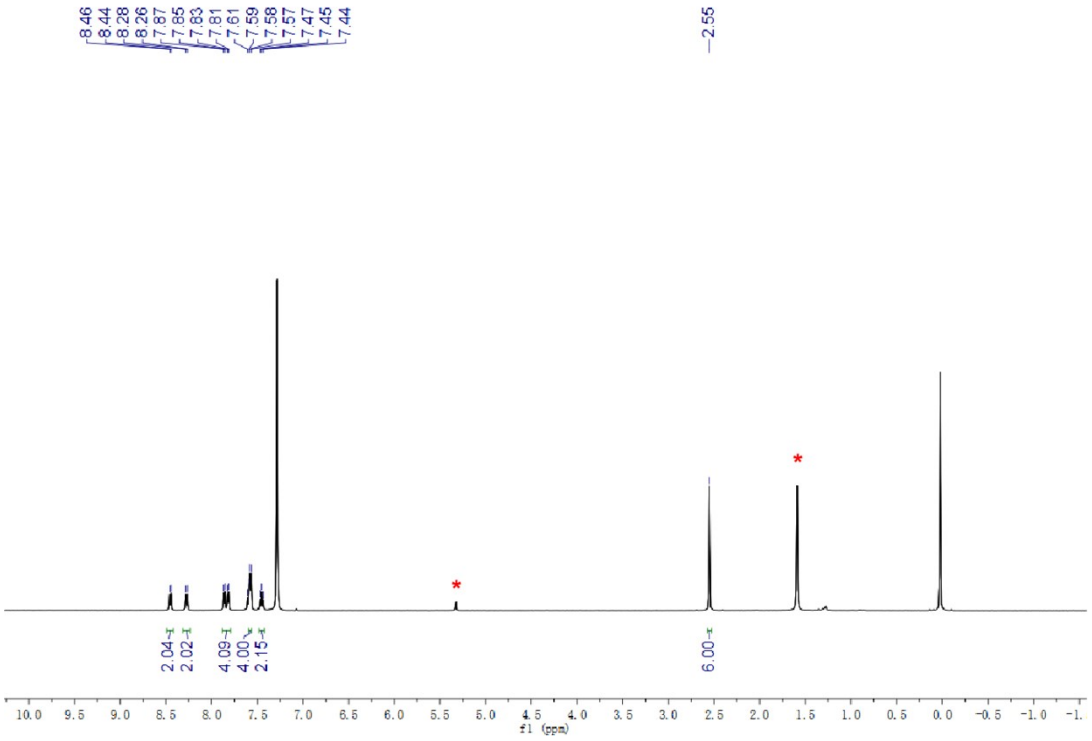

Figure S5. ^{1}H NMR spectrum of *m*-Naph in $CDCl_3$.

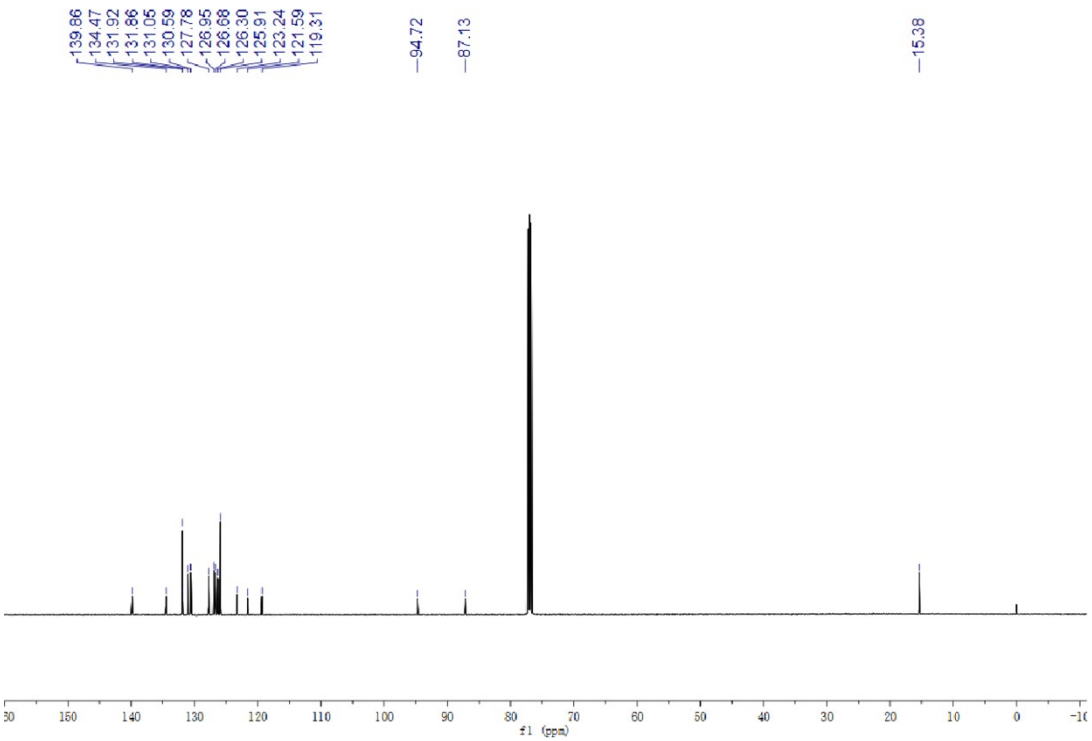

Figure S6. ^{13}C NMR spectrum of *m*-Naph in $CDCl_3$.

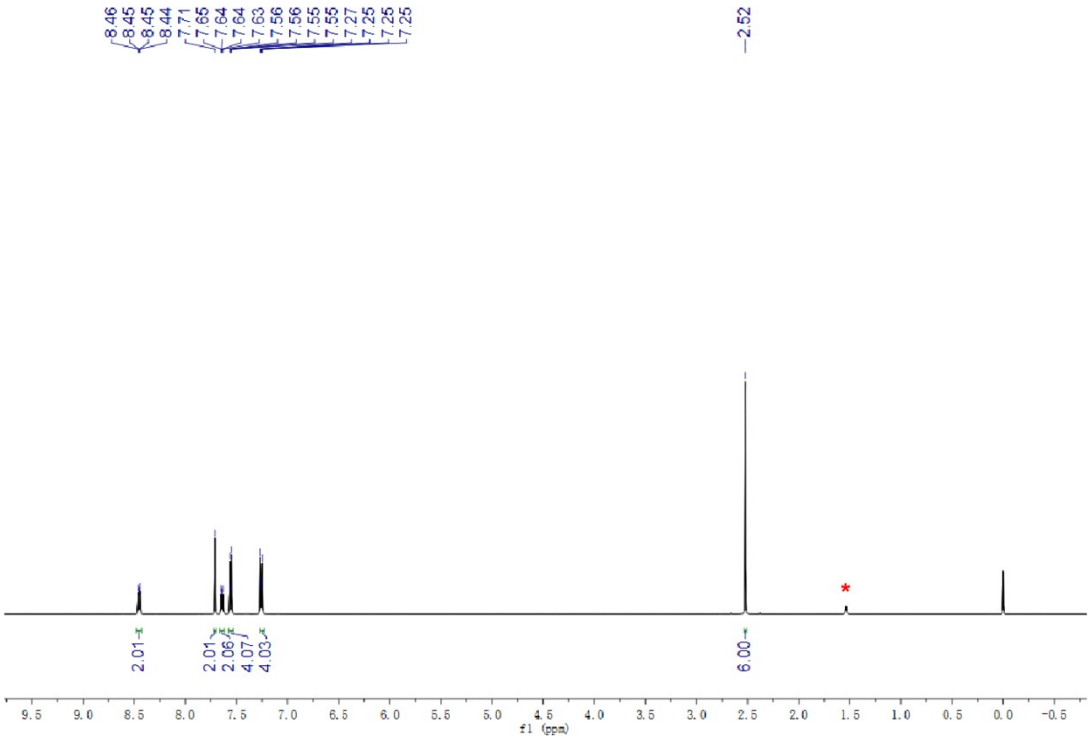

Figure S7. ^{1}H NMR spectrum of *p*-Naph in $CDCl_3$.

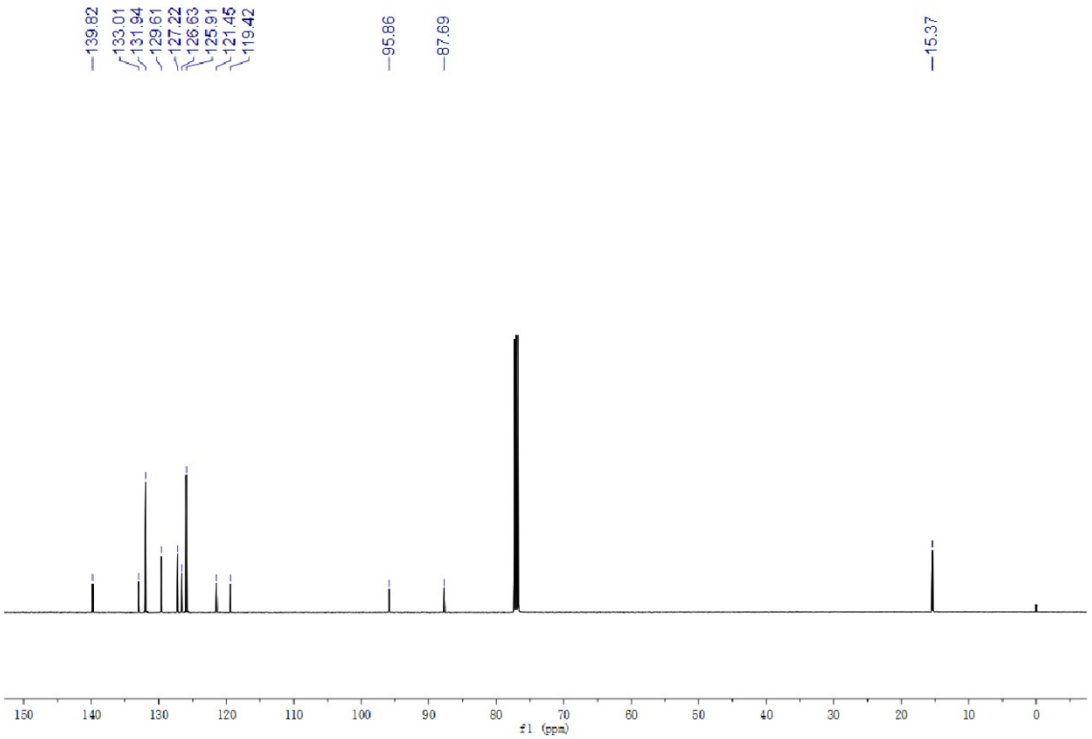

Figure S8. ^{13}C NMR spectrum of *p*-Naph in $CDCl_3$.

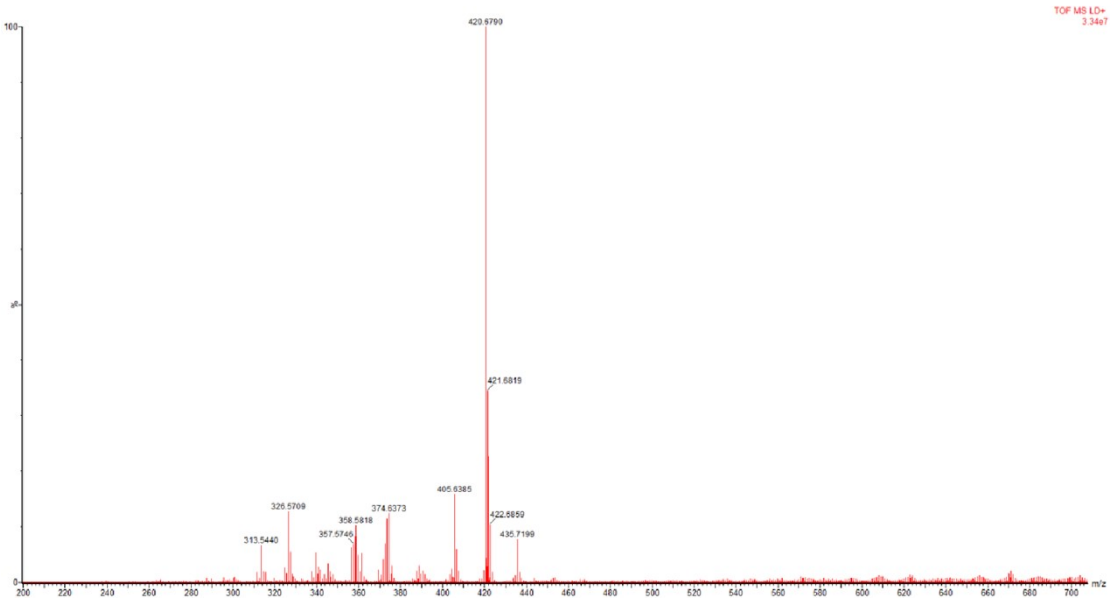

Figure S9. HRMS spectrum of *o*-Naph.

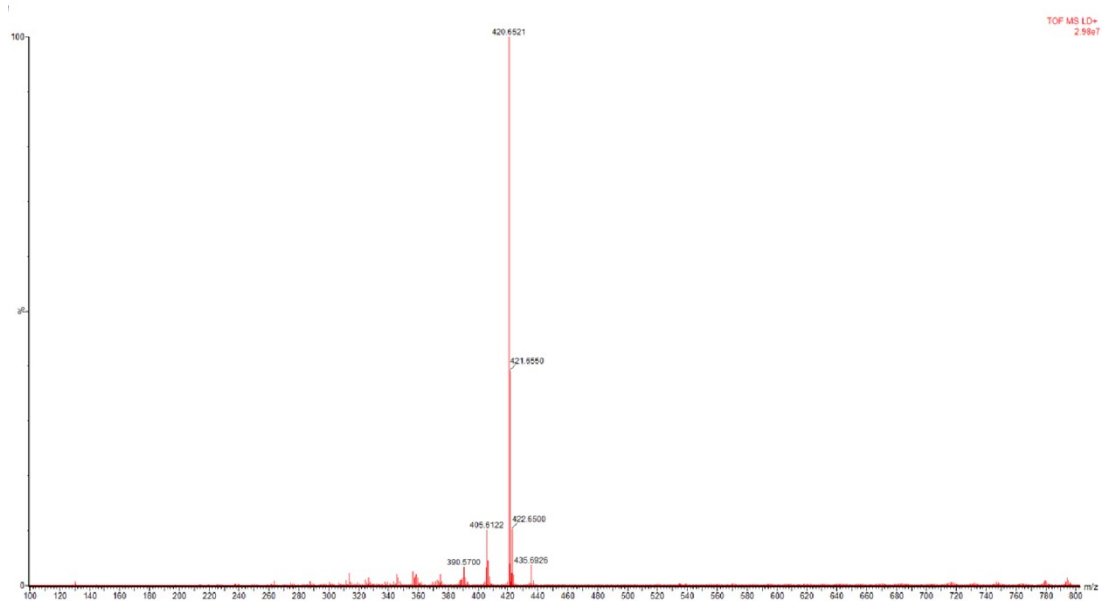

Figure S10. HRMS spectrum of *m*-Naph.

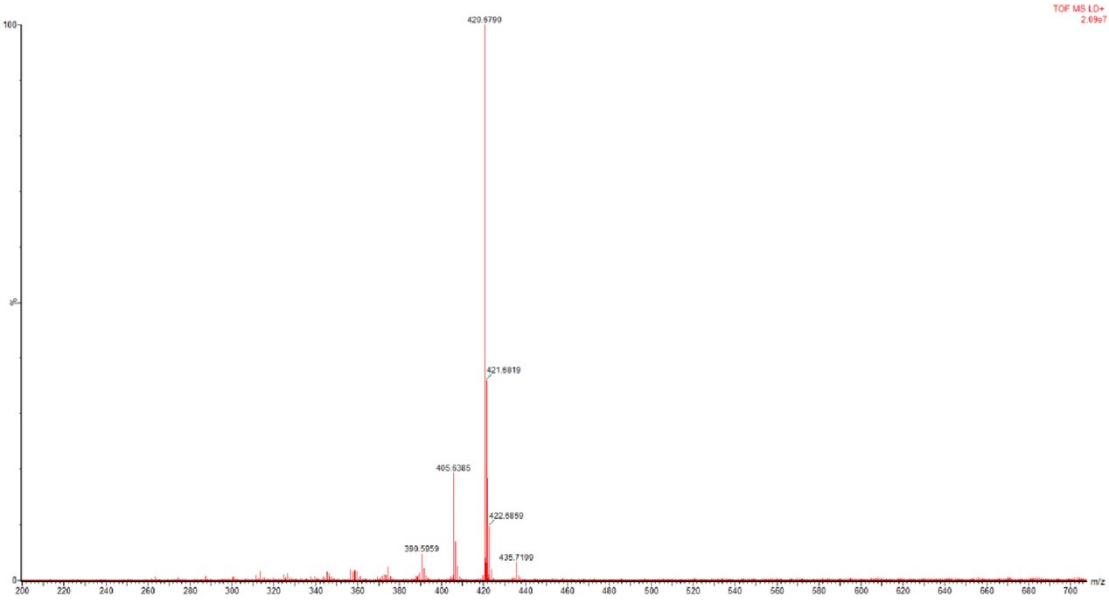

Figure S11. HRMS spectrum of *p*-Naph.

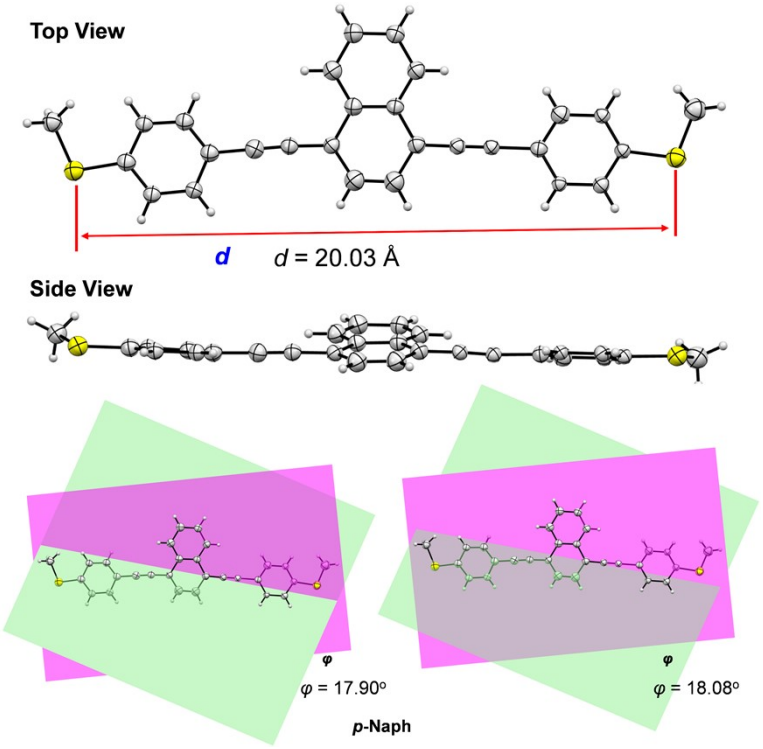

Figure S12. ORTEP drawings of crystal structures of *p*-Naph with torsional angles between peripheral phenyls and naphthalene core and S-S distance.

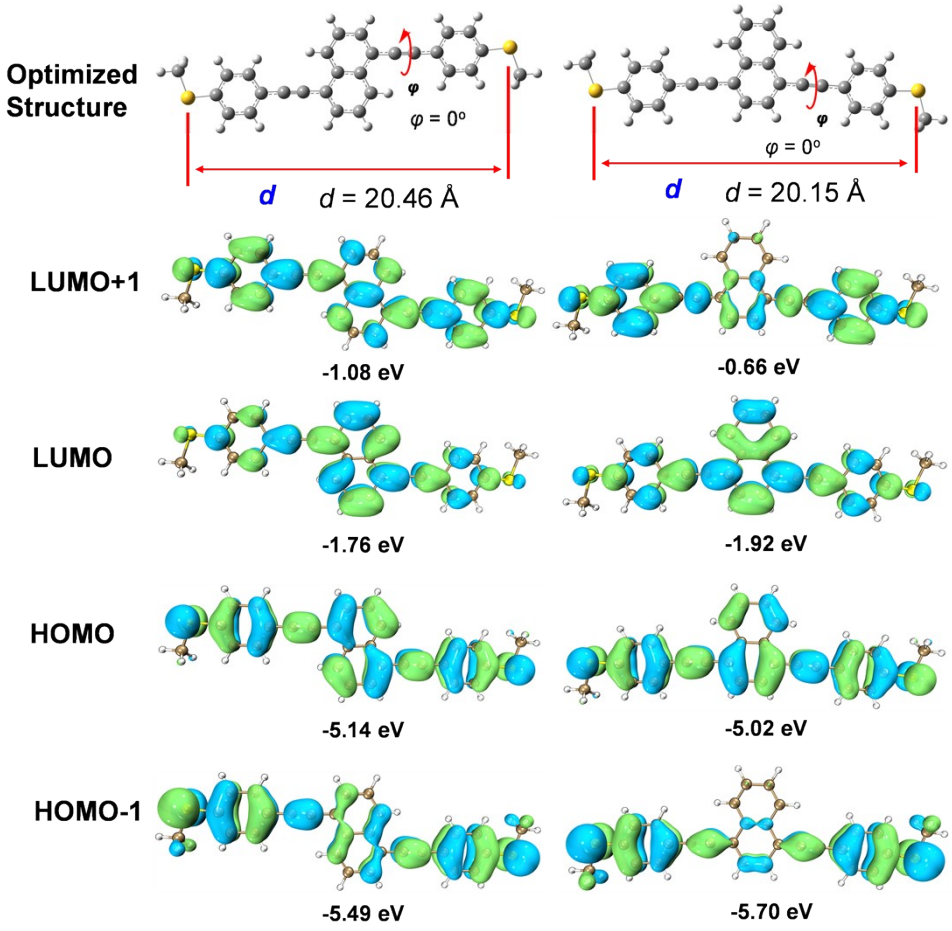

Figure S13. Optimized molecular structures of *m*-Naph and *p*-Naph with torsional angles and calculated S-S distance and spatial distributions of HOMOs and LUMOs of *m*-Naph and *p*-Naph.

Reference

1. M. J. Frisch, G. W. Trucks, H. B. Schlegel, G. E. Scuseria, M. A. Robb, J. R. Cheeseman, G. Scalmani, V. Barone, G. A. Petersson, H. Nakatsuji, X. Li, M. Caricato, A. V. Marenich, J. Bloino, B. G. Janesko, R. Gomperts, B. Mennucci, H. P. Hratchian, J. V. Ortiz, A. F. Izmaylov, J. L. Sonnenberg, Williams, F. Ding, F. Lipparini, F. Egidi, J. Goings, B. Peng, A. Petrone, T. Henderson, D. Ranasinghe, V. G. Zakrzewski, J. Gao, N. Rega, G. Zheng, W. Liang, M. Hada, M. Ehara, K. Toyota, R. Fukuda, J. Hasegawa, M. Ishida, T. Nakajima, Y. Honda, O. Kitao, H. Nakai, T. Vreven, K. Throssell, J. A. Montgomery Jr., J. E. Peralta, F. Ogliaro, M. J. Bearpark, J. J. Heyd, E. N. Brothers, K. N. Kudin, V. N. Staroverov, T. A. Keith, R. Kobayashi, J. Normand, K. Raghavachari, A. P. Rendell, J. C. Burant, S. S. Iyengar, J. Tomasi, M. Cossi, J. M. Millam, M. Klene, C. Adamo, R. Cammi, J. W. Ochterski, R. L. Martin, K. Morokuma, O. Farkas, J. B. Foresman and D. J. Fox,, Gaussian 16, Revision A. 03. Wallingford.

2. T. Lu and F. Chen, J. Comput. Chem., 2012, 33, 580–592.